

Dilution induced magnetic localization in $\text{Rb}(\text{Co}_{1-x}\text{Ni}_x)_2\text{Se}_2$ single crystals

Hui Liu,¹ Mengwu Huo,¹ Chaoxin Huang,¹ Xing Huang,¹ Hualei Sun,¹
Lan Chen,¹ Juping Xu,^{2,3} Wen Yin,^{2,3} Runxia Li,^{4,*} and Meng Wang^{1,†}

¹Center for Neutron Science and Technology, Guangdong Provincial Key Laboratory of Magnetoelectric Physics and Devices, School of Physics, Sun Yat-Sen University, Guangzhou, 510275, China

²Institute of High Energy Physics, Chinese Academy of Sciences, Beijing 100049, China

³Spallation Neutron Source Science Center, Dongguan 523803, China

⁴Materials Science and Engineering, Dongguan University of Technology, Dongguan 523808, China

We report experimental studies on a series of $\text{Rb}(\text{Co}_{1-x}\text{Ni}_x)_2\text{Se}_2$ ($0.02 \leq x \leq 0.9$) powder and single crystal samples using x-ray diffraction, neutron diffraction, magnetic susceptibility, and electronic transport measurements. All compositions are metallic and adopt the body-centered tetragonal structure with $I4/mmm$ space group. Anisotropic magnetic susceptibilities measured on single crystal samples suggest that $\text{Rb}(\text{Co}_{1-x}\text{Ni}_x)_2\text{Se}_2$ undergo an evolution from ferromagnetism to antiferromagnetism, and finally to paramagnetism with increasing Ni concentration. Neutron diffraction measurements on the samples with $x = 0.1, 0.4,$ and 0.6 reveal an A -type antiferromagnetic order with moments lying in the ab plane. The moment size changes from 0.69 ($x = 0.1$) to $2.80\mu_B$ ($x = 0.6$) per Co ions. Our results demonstrate that dilution of the magnetic Co ions by substitution of nonmagnetic Ni ions induces magnetic localization and evolution from itinerant to localized magnetism in $\text{Rb}(\text{Co}_{1-x}\text{Ni}_x)_2\text{Se}_2$.

PACS numbers:

I. INTRODUCTION

Layered transition metal chalcogenides with the ThCr_2Si_2 -type structure show versatile characteristics, such as superconductivity, heavy fermion behavior, and various magnetic orders due to the sensitivity of the magnetic and electronic correlations to the atomic distances and compositions.^{1–8} The iron chalcogenide compounds $A_x\text{Fe}_2\text{Se}_2$ ($A = \text{K}, \text{Rb}, \text{Cs},$ and Tl) exhibit superconductivity with a transition temperature at ~ 30 K.^{9,10} While by inducing iron vacancies, for compositions with $\delta = 0.4$ and 0.5 , $A_x\text{Fe}_{2-\delta}\text{Se}_2$ become insulating and show iron vacancy and antiferromagnetic (AFM) orders.^{11–13} In the insulating states, the Fe^{2+} with fully localized electrons are in a high spin state. The Co-doping in $A_x\text{Fe}_2\text{Se}_2$ suppresses the superconductivity rapidly and induces metallic magnetic ground states.^{8,14–17}

By replacing Fe for Ni, the ANi_2Se_2 compounds show Pauli paramagnetic (PM), multi-band characteristics, and superconductivity with superconducting transition temperatures at $0.8 \sim 3.7$ K.^{18–22} While the isostructural compounds KCo_2Se_2 and RbCo_2Se_2 exhibit ferromagnetic (FM) order with Curie temperatures of $T_C = 74$ and 83 K, respectively.^{8,14} CsCo_2Se_2 is an A -type AFM metal with moments lying in the ab plane.^{16,23} The size of the in-plane ordered moments of Co ions in RbCo_2Se_2 is $\sim 0.60\mu_B$ determined from neutron diffraction measurement, indicating an itinerant origin.¹⁴ As a simple expectation, Ni substitution on the Co sites would progressively tune the ground states of $\text{Rb}(\text{Co}_{1-x}\text{Ni}_x)_2\text{Se}_2$ from FM order to PM state. However, in previous studies of $\text{Tl}(\text{Co}_{1-x}\text{Ni}_x)_2\text{Se}_2$ and $\text{Tl}(\text{Co}_{1-x}\text{Ni}_x)_2\text{S}_2$, the AFM order was found to exist in a large region of the Ni doping level. Although the magnetic order of TlCo_2Se_2 is AFM and that of TlCo_2S_2 is FM.^{24,25} These results indicate

that the effect of Ni substitution on the magnetism in $A(\text{Co}_{1-x}\text{Ni}_x)_2\text{X}_2$ ($X = \text{Se}$ and S) has a unique mechanism, motivating us to explore the magnetic and electronic properties of $\text{Rb}(\text{Co}_{1-x}\text{Ni}_x)_2\text{Se}_2$ single crystals.

In this work, we report detailed studies on the crystallographic, magnetic structure, magnetic susceptibility, and electronic transport properties of $\text{Rb}(\text{Co}_{1-x}\text{Ni}_x)_2\text{Se}_2$ single crystals by utilizing powder x-ray diffraction (XRD), neutron powder diffraction (NPD), magnetic susceptibility, and resistance measurements. We find by increasing the Ni concentration, (1) the FM order transforms to AFM order at around $x = 0.06$, (2) the AFM order extends to the compositions with $x = 0.8$, (3) the anisotropic in-plane and out-of-plane magnetic susceptibilities reverse magnitudes at $x \approx 0.3$, and (4) the $x = 0.9$ compound is paramagnetic. Neutron diffraction measurements reveal that the AFM phase corresponds to a universal A -type magnetic structure with spins aligned in the ab plane. While the moment size is increased from $0.69(2)$ for $x = 0.1$ to $2.80(6)\mu_B$ for $x = 0.6$. The residual resistivity ratio (RRR) shows an intimate relationship with magnetism. The results suggest that the dilution of magnetic Co by nonmagnetic Ni has increased the localization of Co $3d$ electrons. The magnetism evolves from itinerant to localized in the AFM region of the $\text{Rb}(\text{Co}_{1-x}\text{Ni}_x)_2\text{Se}_2$ phase diagram. Spin glass state is also identified in the compounds we explored.

II. EXPERIMENTAL DETAILS

Single crystals of $\text{Rb}(\text{Co}_{1-x}\text{Ni}_x)_2\text{Se}_2$ with compositions of $x = 0.02, 0.04, 0.06, 0.08, 0.1, 0.2, 0.3, 0.4, 0.5, 0.6, 0.7, 0.8,$ and 0.9 were synthesized by the Bridgman method with two-step reacting. $\text{Co}_{1-x}\text{Ni}_x\text{Se}$ precursors

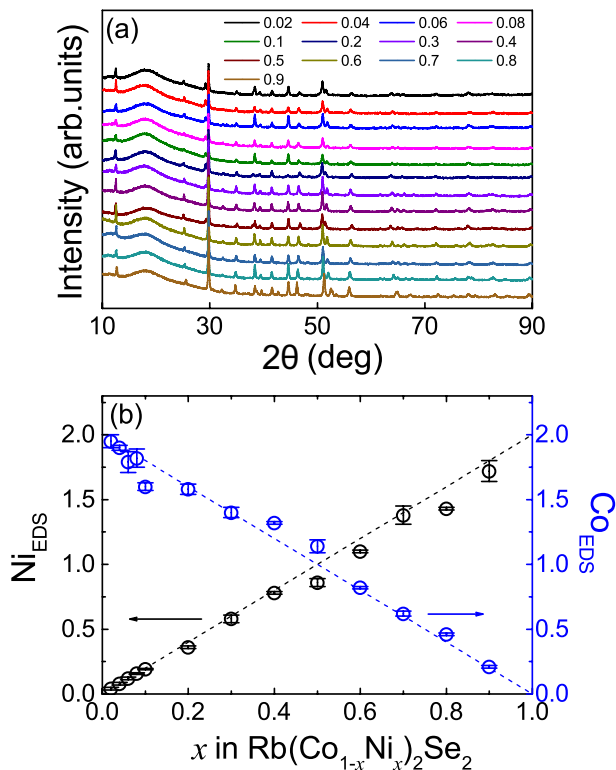


FIG. 1: (a) XRD patterns of $\text{Rb}(\text{Co}_{1-x}\text{Ni}_x)_2\text{Se}_2$ powder samples with $0.02 \leq x \leq 0.9$. (b) EDS determined concentrations of Ni and Co as a function of the nominal concentration of Ni, x . Error bars are the uncertainty of the EDS results.

were prepared by using Ni, Co powders, and Se shots to react at 500°C in an evacuated quartz tube. The process was repeated two times for homogeneity. Then, stoichiometric Rb ingot and $\text{Co}_{1-x}\text{Ni}_x\text{Se}$ powders were placed in an aluminum crucible and sealed in an evacuated quartz tube. The mixtures were heated to 1070°C and kept for 10 h. After the samples were slowly cooled down to 700°C at a rate of $3.7^\circ\text{C}/\text{h}$, the furnace was shut down.²² We obtained plate-like single crystals with a typical size of $5 \times 5 \times 1 \text{ mm}^3$. As the Ni content increases, the samples have a metallic luster with colors from golden to pink. All samples are sensitive to oxygen and moisture. They were saved and handled in an argon-filled glove box.

Powder XRD measurements were conducted on an x-ray diffractometer (Empyrean) at 300 K. NPD experiment was carried out on the multi-physics instrument (MPI) installed at the China Spallation Neutron Source (CSNS). Powder samples ground from single crystals of $\text{Rb}(\text{Co}_{1-x}\text{Ni}_x)_2\text{Se}_2$ with $x = 0.1, 0.4, \text{ and } 0.6$ were sealed in cylindrical vanadium cans with helium atmosphere and measured at 5, 50, and 200 K. NPD data were refined by employing the Rietveld method using the FULLPROF Suite software.^{26,27} The composition analysis was conducted on an energy dispersive x-ray spectroscopy (EDS) (EVO, Zeiss). Resistance, dc, and ac susceptibility were measured on a commercial physical property measurement system (PPMS, Quantum Design). The in-plane

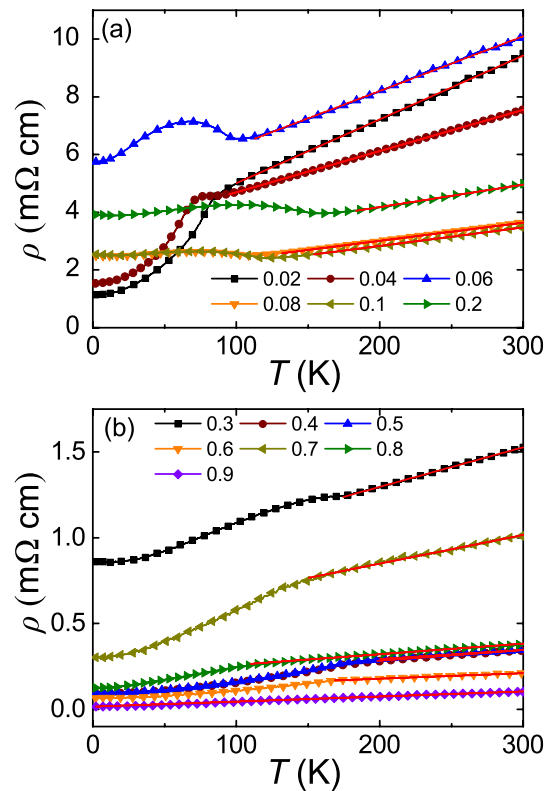


FIG. 2: Temperature dependence of the in-plane resistivity $\rho_{ab}(T)$ for $\text{Rb}(\text{Co}_{1-x}\text{Ni}_x)_2\text{Se}_2$ with (a) $0.02 \leq x \leq 0.2$ and (b) $0.3 \leq x \leq 0.9$. The red-solid lines are linear fits to the resistivity above the magnetic transition temperature.

resistivity measurements were performed using the standard four-probe method.

III. RESULTS AND DISCUSSION

Figure 1(a) shows powder XRD patterns at room temperature for the compositions of $\text{Rb}(\text{Co}_{1-x}\text{Ni}_x)_2\text{Se}_2$ ($0.02 \leq x \leq 0.9$). The XRD patterns can be fitted well by the tetragonal ThCr_2Si_2 -type structure with the space group $I4/mmm$. The fitted lattice constants for different compositions do not show a regular change, consistent with the expectation for the approximate ionic radii of Co and Ni. The average lattice parameters a and c from XRD measurements are $3.902(3)$ and $14.12(2) \text{ \AA}$, respectively. The actual compositions determined by the EDS for single crystals are plotted in Fig. 1(b). The content of Se was normalized to be 2 in the analysis. The linear relationships between the nominal and actual contents of Ni and Co suggest that the substitution is successful for all compositions.

The resistivity $[\rho_{ab}(T)]$ measured in the ab -plane on single crystals of $\text{Rb}(\text{Co}_{1-x}\text{Ni}_x)_2\text{Se}_2$ in the temperature range from 2 to 300 K is shown in Fig. 2. All of the samples display metallic behavior. The resistivity decreases linearly as decreasing temperature before a drop

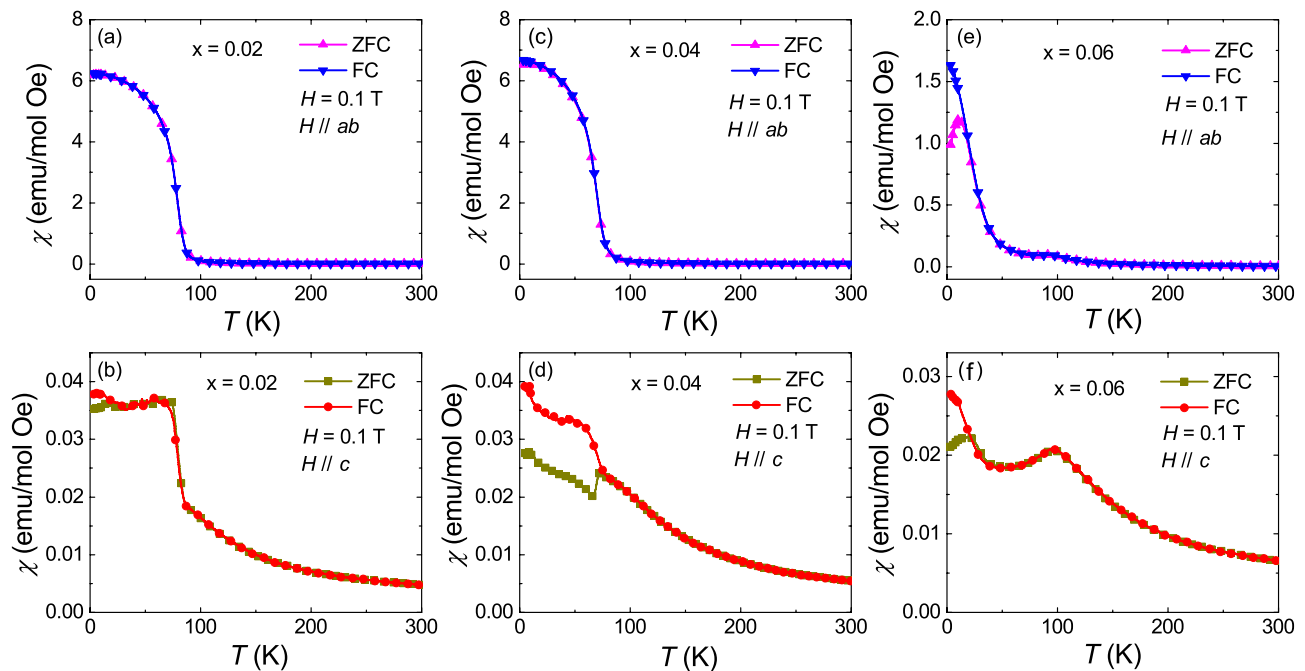


FIG. 3: Temperature dependence of the magnetic susceptibilities $\chi(T)$ for $\text{Rb}(\text{Co}_{1-x}\text{Ni}_x)_2\text{Se}_2$ ($x = 0.02, 0.04,$ and 0.06), measured in ZFC and FC conditions with $H = 0.1$ T. The magnetic fields are parallel to the ab plane in (a), (c), and (e), and parallel to the c axis in (b), (d), and (f).

appears at 86 and 72 K for the compounds with $x = 0.02$ and 0.04 , respectively [Fig. 2(a)]. The drop in resistivity could be attributed to a FM transition, as observed in FM RbCo_2Se_2 and $\text{Tl}_{1-x}\text{K}_x\text{Co}_2\text{Se}_2$, which can be understood by suppression of the magnetic scattering on conduction electrons in the FM state.^{4,14} The anomalies can also be observed in the resistivity of $\text{Rb}(\text{Co}_{1-x}\text{Ni}_x)_2\text{Se}_2$ with $x = 0.06, 0.08, 0.1, 0.2,$ and 0.3 at higher temperatures. However, the resistivity shows a hump below the magnetic transition reminiscent of the behavior in CsCo_2Se_2 , which undergoes an AFM transition at low temperatures.²⁸ Thus, the Ni substitution on the Co site may induce a FM to AFM ground state transition. The Ni ions exhibit a paramagnetic characteristic in RbNi_2Se_2 .²² Further increasing the Ni content, the magnetic scattering would be reduced due to the decrease of the magnetic Co ions. The anomalies in resistivity for the compounds with $0.4 \leq x \leq 0.8$ indeed become weaker, as shown in Fig. 2(b). For the composition with $x = 0.9$, the $\rho_{ab}(T)$ does not show any anomaly in the measured temperature range, similar to RbNi_2Se_2 .

To investigate the magnetic properties, we measured the magnetic susceptibilities [$\chi(T)$] for all the compounds, as shown in Figs. 3 and 4. Figure 3 shows the $\chi(T)$ under zero-field-cooled (ZFC) and field-cooled (FC) conditions for the $\text{Rb}(\text{Co}_{1-x}\text{Ni}_x)_2\text{Se}_2$ crystals with $x = 0.02, 0.04,$ and 0.06 . The susceptibility data were collected with the magnetic field applied along the ab plane [χ_{ab}] and the c axis [χ_c], respectively. The abrupt enhancement of χ_{ab} below 100 K reveals the development of a long-range FM order, as shown in Fig. 3(a), (c), and

(e) for the compounds $x = 0.02, 0.04,$ and 0.06 . The enhancement could also be observed on the χ_c . However, the strength of the magnetic response within the layer [χ_{ab}] shows an order of magnitude larger than that of the out-of-layer [χ_c], yielding that the ferromagnetically ordering moments are aligned in the ab plane. For the compound with $x = 0.06$, the out-of-plane susceptibility displays a cusp-like peak around 96 K [Fig. 3(f)], in contrast to the in-plane FM behavior, implying that an AFM order may occur along the c axis.

The magnetic susceptibilities for $x = 0.08, 0.1, 0.2, 0.3, 0.4, 0.5, 0.7, 0.8,$ and 0.9 are shown in Figs. 4(a)-4(i) with $H \parallel ab$ and $H \parallel c$, respectively. The cusp-like anomalies are more obvious in the susceptibilities of $\text{Rb}(\text{Co}_{1-x}\text{Ni}_x)_2\text{Se}_2$ with $0.08 \leq x \leq 0.8$. The magnitudes of χ_{ab} and χ_c are comparable and consistent with an AFM order. Interestingly, there is an obvious magnitude change between the χ_{ab} and χ_c in the composition range of $x = 0.08$ to $x = 0.8$, where the magnitude reverses at $x = 0.3$. It is difficult to determine the origin of the changes in magnetic susceptibility because of the unknown AFM order and the substitution of the magnetic Co ions.

Comparing the ZFC to FC magnetic susceptibilities, a pronounced bifurcation can be observed below a transition temperature for the compositions with $0.06 \leq x \leq 0.9$. The irreversible behavior implies a spin-glass (SG) state, which may be related to the doping of the nonmagnetic Ni ions. The frequency-dependent ac susceptibility measurements were adopted to verify the SG state for the compound with $x = 0.2$. The magnetic field was applied parallel to the ab plane. As shown in the inset of

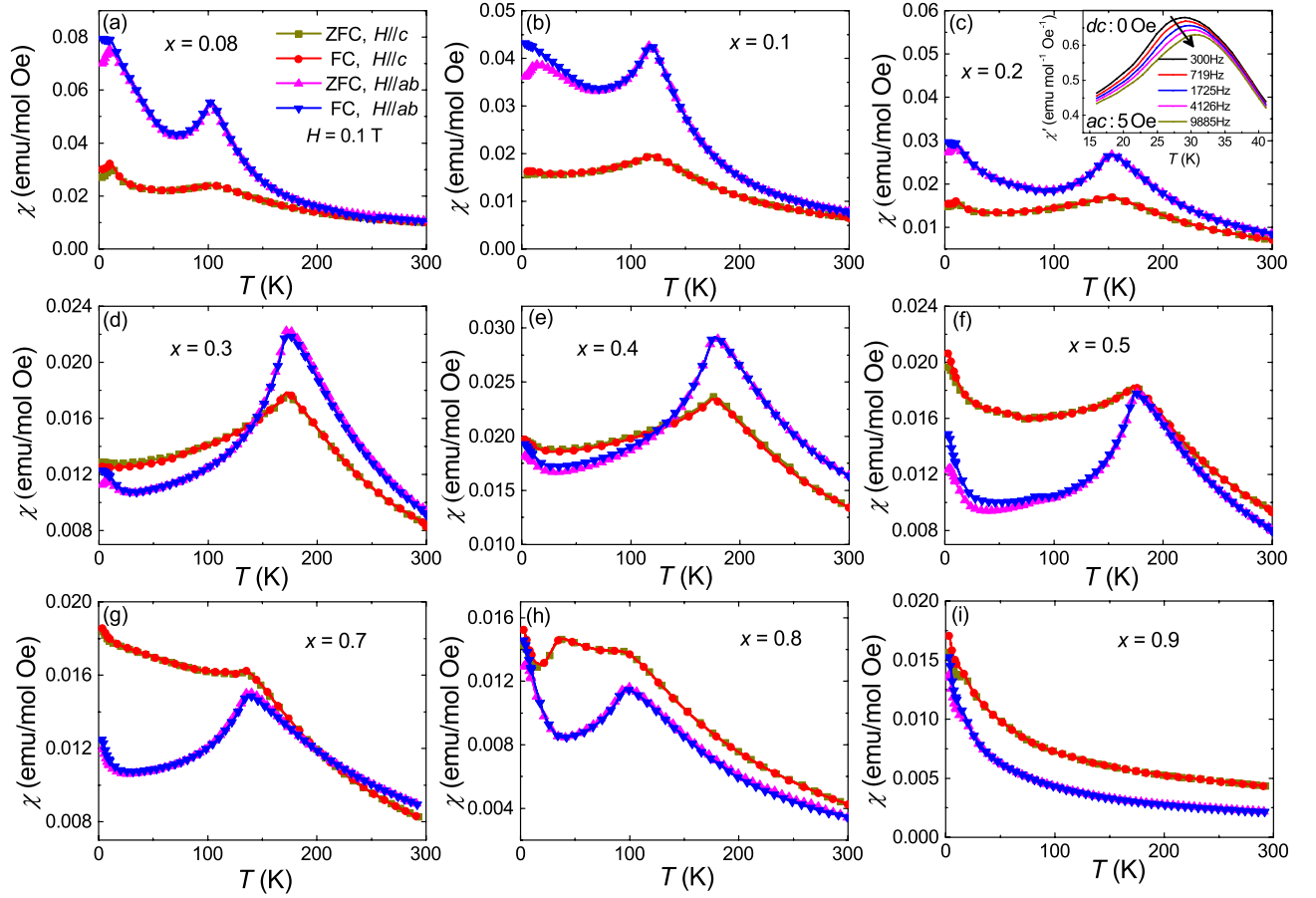


FIG. 4: Temperature dependence of $\chi(T)$ measured in ZFC and FC conditions for $H \parallel ab$ and $H \parallel c$ with $H = 0.1$ T for $\text{Rb}(\text{Co}_{1-x}\text{Ni}_x)_2\text{Se}_2$ with (a) $x = 0.08$, (b) $x = 0.1$, (c) $x = 0.2$, (d) $x = 0.3$, (e) $x = 0.4$, (f) $x = 0.5$, (g) $x = 0.7$, (h) $x = 0.8$, and (i) $x = 0.9$. The Inset in (c) is the temperature dependence of the $\chi'(T)$ measured at various ac magnetic field frequencies between 300 and 9885 Hz for the compound with $x = 0.20$. The ac magnetic field is parallel to the ab plane. The arrow indicates a shift in the freezing temperatures.

Fig. 4(c), the real part of the ac susceptibilities $\chi'(T)$ exhibit a clear frequency dependence. With increasing frequency, the peak position shifts to higher temperatures while the peak amplitude decreases. The Mydosh parameter (δT_f) represents the relative shift in freezing temperature per decade of frequency, which can be calculated by $\delta T_f = \Delta T_f / (T_f \Delta \log f)$.²¹ The spin freezing temperature T_f is defined by the peak position from the ZFC curve. The obtained δT_f value is 0.031, consistent with the values of $0.0045 \leq \delta T_f \leq 0.08$ for a typical SG state. For the compound with $x = 0.9$ in Fig. 4(i), the magnetic transition disappears in the temperature dependence of susceptibility. The $\chi(T)$ curves exhibit the Pauli PM behavior without long-range magnetic order, similar to the characteristic of RbNi_2Se_2 .²²

To obtain accurate magnetic structures, NPD data were collected for samples with $x = 0.1, 0.4$, and 0.6 . The reflection patterns and the Rietveld method refinements are shown in Fig. 5. By comparing the data at 5, 50, and 200 K, a magnetic peak at $d = 14.2$ Å can be identified. The magnetic peak can be indexed with

the propagation vector $\mathbf{k} = [1, 0, 0]$ in the notation of the $I4/mmm$ space group with A -type AFM order, as shown in Fig. 6(c). The magnetic diffraction peak observed at $d = 14.2$ Å corresponds to the magnetic Bragg reflection $(H, K, L) = (001)$. Here, we assume the magnetism arising from the Co ions. The ordered moments are refined to be 0.69(2), 1.98(4), and 2.80(6) μ_B per Co at 5 K for the compounds with $x = 0.1, 0.4$, and 0.6 , respectively. The increased ordered moment for the $x = 0.6$ compound is close to the fully localized high spin state of Co^{2+} with $S = 3/2$.

Knowing the A -type magnetic order and moment sizes for the compounds with $0.08 \leq x \leq 0.8$, the evolution of the magnetic susceptibilities can be understood. By increasing the content of Ni, the magnetism evolves from itinerant to localized, accompanied by the enhancement of the ordered moment size. The AFM intralayer coupling between the FM layers will be increased accordingly. For the compounds with $x = 0.08, 0.1$, and 0.2 , the χ_{ab} sharply drops at the magnetic transition temperature T_N . The χ_c has a weak temperature dependence

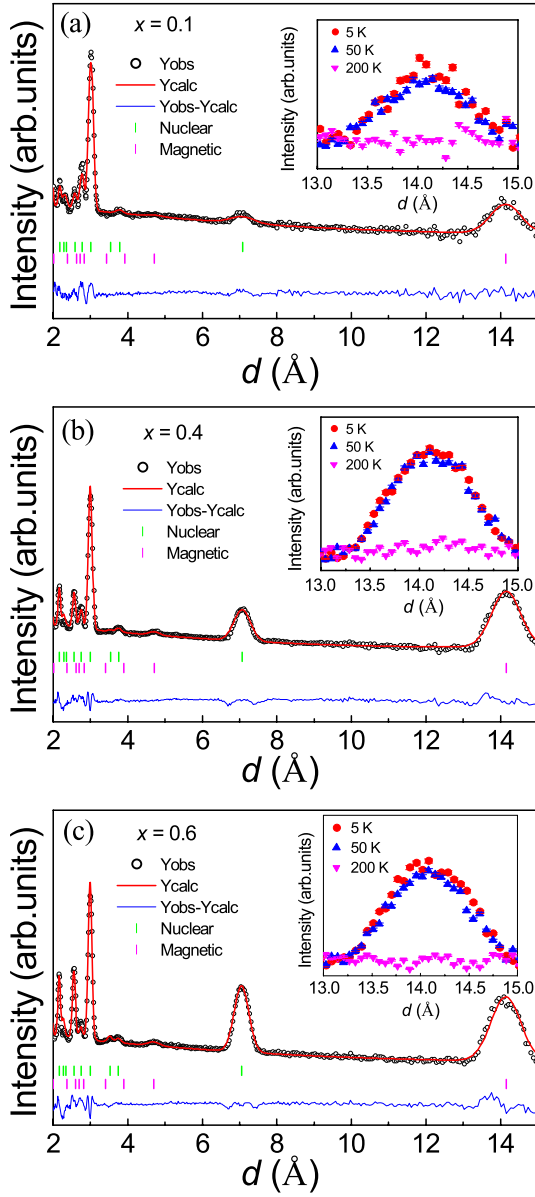


FIG. 5: NPD patterns for $\text{Rb}(\text{Co}_{1-x}\text{Ni}_x)_2\text{Se}_2$ at 5 K with (a) $x = 0.1$, (b) $x = 0.4$, and (c) $x = 0.6$. The insets are temperature dependence of the magnetic diffraction peak corresponding to the (001) reflection at 5, 50, and 200 K. The errors in the insets indicate one standard deviation.

below T_N , typically conforming the *A*-type AFM structure with the magnetic moments lying along the *ab*-plane. The value of in-plane susceptibility χ_{ab} is enhanced by the *ab*-plane collinear ferromagnetic layers, larger than the out-of-plane susceptibility χ_c . A similar magnetic structure has been reported in CsCo_2Se_2 , which exhibits the approximate magnetic behavior.^{8,28} When $x = 0.3$ and 0.4 , the susceptibilities exhibit a crossover between the χ_{ab} and χ_c . Such a crossover could be ascribed to the dilution of the magnetic Co ions in the *ab* plane and the enhancement of the AFM intralayer coupling.

By combining the experimental results on

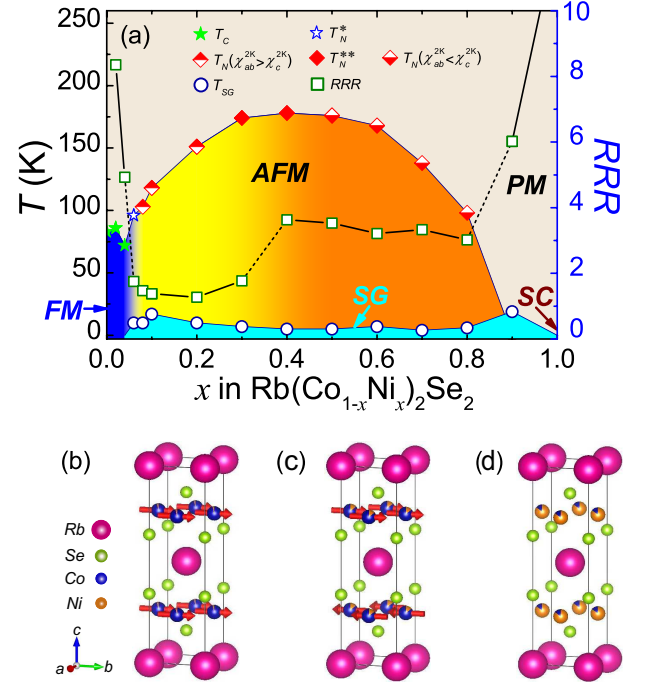


FIG. 6: (a) A phase diagram of $\text{Rb}(\text{Co}_{1-x}\text{Ni}_x)_2\text{Se}_2$ with the FM transition temperature [T_C], AFM transition temperature [T_N , T_N^* , T_N^{**}], spin glass transition temperature [T_{SG}], and the residual resistivity ratio [RRR]. T_N^* represents the AFM transition temperature for the critical concentration $x = 0.6$ with FM behavior on χ_{ab} and AFM behavior on χ_c . T_N^{**} is the AFM transition temperature for $x = 0.3$ and 0.4 , where the anisotropic susceptibility curve has a crossover below T_N . Schematic diagrams of (b) the FM structure, (c) the AFM structure, and (d) the PM structure in the phase diagram.

$\text{Rb}(\text{Co}_{1-x}\text{Ni}_x)_2\text{Se}_2$, we construct a comprehensive phase diagram in Fig. 6(a), summarizing the evolutions of the magnetic order, spin glass state, and RRR as a function of the Ni content x . For $x = 0.02$ and 0.04 , the anisotropic magnetic susceptibilities reveal a FM order with moments aligned in the *ab* plane, as shown in Fig. 6(b). Both the FM and AFM transitions could be identified in the compound with $x = 0.06$, suggesting that the FM to AFM transformation is a first-order transition and $x = 0.06$ is close to the critical composition. The AFM structure is shown in Fig. 6(c). For the compounds with AFM order, the magnetic susceptibility changes from $\chi_{ab} > \chi_c$ to $\chi_{ab} < \chi_c$ at the compositions with $x = 0.3$ and 0.4 , resulting from the dilution of the magnetic Co ions and localization of the magnetic moments. The AFM transition vanishes from the susceptibility measurements for the compound with $x = 0.9$ [Fig. 6(d)]. The SG transition temperature [T_{SG}] is defined as the bifurcation point between the ZFC and FC susceptibilities. The T_{SG} and RRR for each composition are plotted in Fig. 6(a). The evolution of the electronic behavior (RRR) is strongly correlated with the magnetic order. The abrupt increase of RRR in the AFM region could be attributed

to the enhancement of the localization of Co ions. To further understand the nature of magnetic and transport properties, angle-resolved photoemission spectroscopy studies on the electronic band structures are required.

IV. SUMMARY

In conclusion, we have grown the single crystals of $\text{Rb}(\text{Co}_{1-x}\text{Ni}_x)_2\text{Se}_2$ with $0.02 \leq x \leq 0.9$ and comprehensively investigated the physical properties via the XRD, EDS, NPD, magnetic susceptibility, and electronic transport methods. By combining these results, we present a phase diagram of $\text{Rb}(\text{Co}_{1-x}\text{Ni}_x)_2\text{Se}_2$. All compositions adopt the space group $I4/mmm$ and show a slight difference in lattice parameters. The magnetism evolves from FM to AFM, then to Pauli paramagnetism with increasing the concentration of Ni. The electronic transport behaviors are closely correlated with the magnetic order. The magnetic structure in the AFM region is confirmed

to be the A -type AFM order by NPD. The AFM moment size is increased significantly as increasing the Ni concentration, demonstrating that the magnetic moments of Co ions become more localized as the dilution effect by the Ni substitution.

V. ACKNOWLEDGMENTS

Work was supported by the Guangdong Basic and Applied Basic Research Foundation (Grants No. 2021B1515120015, 2020B151520065), the National Natural Science Foundation of China (Grant No. 12174454), the Guangzhou Basic and Applied Basic Research Foundation (Grant No. 202201011123), Guangdong Provincial Key Laboratory of Magnetoelectric Physics and Devices (Grant No. 2022B1212010008), and National Key Research and Development Program of China (Grant No. 2019YFA0705702).

-
- * Electronic address: 5327368@qq.com
 † Electronic address: wangmeng5@mail.sysu.edu.cn
- ¹ P. Dai, *Reviews of Modern Physics* **87**, 855 (2015), ISSN 0034-6861, 1503.02340, URL <https://link.aps.org/doi/10.1103/RevModPhys.87.855>.
 - ² P. Gegenwart, Q. Si, and F. Steglich, *Nat. Phys.* **4**, 186 (2008), ISSN 1745-2473, 0712.2045, URL <http://www.nature.com/articles/nphys892>.
 - ³ R. Berger, M. Fritzsche, A. Broddefalk, P. Nordblad, and B. Malaman, *Journal of Alloys and Compounds* **343**, 186 (2002), ISSN 09258388, URL <https://linkinghub.elsevier.com/retrieve/pii/S092583880200115x>.
 - ⁴ G. Huan and M. Greenblatt, *J. Less Common Met.* **156**, 247 (1989), ISSN 00225088, URL <https://linkinghub.elsevier.com/retrieve/pii/0022508889000421>.
 - ⁵ S. Ronneteg, R. Berger, and G. André, *Journal of Magnetism and Magnetic Materials* **322**, 681 (2010), ISSN 03048853, URL <https://linkinghub.elsevier.com/retrieve/pii/S03048853090105x>.
 - ⁶ K. S. V. L. Narasimhan, V. U. S. Rao, R. L. Bergner, and W. E. Wallace, *J. Appl. Phys.* **46**, 4957 (1975), ISSN 0021-8979, URL <http://aip.scitation.org/doi/10.1063/1.321480>.
 - ⁷ J. J. Ying, Y. J. Yan, A. F. Wang, Z. J. Xiang, P. Cheng, G. J. Ye, and X. H. Chen, *Physical Review B* **85**, 214414 (2012), ISSN 1098-0121, URL <https://link.aps.org/doi/10.1103/PhysRevB.85.214414>.
 - ⁸ J. Yang, B. Chen, H. Wang, Q. Mao, M. Imai, K. Yoshimura, and M. Fang, *Physical Review B* **88**, 064406 (2013), ISSN 1098-0121, URL <https://link.aps.org/doi/10.1103/PhysRevB.88.064406>.
 - ⁹ J. Guo, S. Jin, G. Wang, S. Wang, K. Zhu, T. Zhou, M. He, and X. Chen, *Physical Review B* **82**, 180520(R) (2010), ISSN 10980121, 1012.2924.
 - ¹⁰ M. Fang, H. Wang, C. Dong, Z. Li, C. Feng, J. Chen, and H. Q. Yuan, *Europhysics Letters* **94**, 27009 (2010), 1012.5236, URL <http://arxiv.org/abs/1012.5236>.
 - ¹¹ W. Bao, Q. Huang, G. F. Chen, M. a. Green, D. M. Wang, J. B. He, X. Q. Wang, and Y. Qiu, *Chinese Physics Letters* **28**, 086104 (2011), ISSN 0256-307X, 1102.0830, URL <http://arxiv.org/abs/1102.0830>.
 - ¹² J. Zhao, H. Cao, E. Bourret-Courchesne, D. H. Lee, and R. J. Birgeneau, *Physical Review Letters* **109**, 267003 (2012), ISSN 00319007, 1205.5992.
 - ¹³ M. Wang, M. Yi, W. Tian, E. Bourret-Courchesne, and R. J. Birgeneau, *Physical Review B* **93**, 075155 (2016), ISSN 2469-9950, 1508.04482, URL <https://link.aps.org/doi/10.1103/PhysRevB.93.075155>.
 - ¹⁴ J. Huang, Z. Wang, H. Pang, H. Wu, H. Cao, S.-K. Mo, A. F. Kemper, M. Wang, M. Yi, et al., *Physical Review B* **103**, 165105 (2021), ISSN 2469-9950, URL <https://link.aps.org/doi/10.1103/PhysRevB.103.165105>.
 - ¹⁵ D. Lizárraga, S. Ronneteg, R. Berger, A. Bergman, P. Mohn, O. Eriksson, and L. Nordström, *Physical Review B* **70**, 024407 (2004), ISSN 1098-0121, URL <https://link.aps.org/doi/10.1103/PhysRevB.70.024407>.
 - ¹⁶ J. Sheng, W. Luo, J. Wang, W. Bao, J. Yang, M. Fang, and S. A. Danilkin, *Chinese Physics B* **27**, 117401 (2018), ISSN 1674-1056, 1811.00243, URL <https://iopscience.iop.org/article/10.1088/1674-1056/27/11/117401>.
 - ¹⁷ H. Ryu, K. Wang, M. Opacic, N. Lazarevic, J. B. Warren, Z. V. Popovic, E. S. Bozin, and C. Petrovic, *Physical Review B* **92**, 174522 (2015), ISSN 1550235X.
 - ¹⁸ H. Lei, M. Abeykoon, K. Wang, E. S. Bozin, H. Ryu, D. Graf, J. B. Warren, and C. Petrovic, *Journal of Physics-Condensed Matter* **26**, 015701 (2014), ISSN 0953-8984, URL <https://iopscience.iop.org/article/10.1088/0953-8984/26/1/015701>.
 - ¹⁹ H. Chen, J. Yang, C. Cao, L. Li, Q. Su, B. Chen, H. Wang, Q. Mao, B. Xu, J. Du, et al., *Superconductor Science and Technology* **29**, 045008 (2016), ISSN 13616668, 1508.05167.
 - ²⁰ H. Wang, C. Dong, Q. Mao, R. Khan, X. Zhou, C. Li, B. Chen, J. Yang, Q. Su, and M. Fang, *Physical Review Letters* **111**, 207001 (2013), ISSN 0031-9007, URL <https://link.aps.org/doi/10.1103/PhysRevLett.111.207001>.

- ²¹ H. Ryu, M. Abeykoon, K. Wang, H. Lei, N. Lazarevic, J. B. Warren, E. S. Bozin, Z. V. Popovic, and C. Petrovic, *Insulating and metallic spin glass in Ni-doped $KxFe_{2-y}Se_2$ single crystals* (2015), URL <https://link.aps.org/doi/10.1103/PhysRevB.91.184503>.
- ²² H. Liu, X. Hu, H. Guo, X.-k. Teng, H. Bu, Z. Luo, L. Li, Z. Liu, M. Huo, F. Liang, et al., *Physical Review B* **106**, 094511 (2022), ISSN 2469-9950, URL <https://link.aps.org/doi/10.1103/PhysRevB.106.094511>.
- ²³ F. Von Rohr, A. Krzton-Maziopa, V. Pomjakushin, H. Grundmann, Z. Guguchia, W. Schnick, and A. Schilling, *Journal of Physics Condensed Matter* **28**, 276001 (2016), ISSN 1361648X, 1605.01113.
- ²⁴ A. Newmark, G. Huan, M. Greenblatt, and M. Croft, *Solid State Communications* **71**, 1025 (1989), ISSN 00381098, URL <https://linkinghub.elsevier.com/retrieve/pii/00381098990584>.
- ²⁵ G. Huan, M. Greenblatt, and K. Ramanujachary, *Solid State Communications* **71**, 221 (1989), ISSN 00381098, URL <https://linkinghub.elsevier.com/retrieve/pii/00381098990406>.
- ²⁶ H. M. Rietveld, *J. Appl. Crystallogr.* **2**, 65 (1969), ISSN 00218898, URL <https://scripts.iucr.org/cgi-bin/paper?S0021889869006558>.
- ²⁷ J. Rodríguez-Carvajal, *Physica B-Condensed Matter* **192**, 55 (1993), ISSN 09214526, URL <https://linkinghub.elsevier.com/retrieve/pii/092145269390108>.
- ²⁸ J. Yang, W. Yang, Q. Zhu, B. Chen, H. Wang, Q. Mao, J. Du, Z. Lou, and M. Fang, *Journal of Magnetism and Magnetic Materials* **474**, 70 (2019), ISSN 03048853, URL <https://doi.org/10.1016/j.jmmm.2018.11.002>.